ISSN 1674-1056
http://cpb.iphy.ac.cn
http://iopscience.iop.org/cpb
中国物理 B
Chinese Physics
中国物理
Chinese Physics B

# Influences of grain size and microstructure on optical properties of microcrystalline diamond films

Jia-Le Wang(王家乐), Cheng-Ke Chen(陈成克), Xiao Li(李晓), Mei-Yan Jiang(蒋梅燕), Xiao-Jun Hu(胡晓君)

**Citation:**Chin. Phys. B . 2020, 29(1): 018103 . **doi:** 10.1088/1674-1056/ab593d
Journal homepage: http://cpb.iphy.ac.cn; http://iopscience.iop.org/cpb

**What follows is a list of articles you may be interested in**

---

## High-gradient magnetic field-controlled migration of solutes and particles and their effects on solidification microstructure: A review

Tie Liu(刘铁), Qiang Wang(王强), Yi Yuan(苑轶), Kai Wang(王凯), Guojian Li(李国建)
Chin. Phys. B . 2018, 27(11): 118103 . **doi:** 10.1088/1674-1056/27/11/118103

## Material microstructures analyzed by using gray level Co-occurrence matrices

Yansu Hu(胡延苏), Zhijun Wang(王志军), Xiaoguang Fan(樊晓光), Junjie Li(李俊杰), Ang Gao(高昂)
Chin. Phys. B . 2017, 26(9): 098104 . **doi:** 10.1088/1674-1056/26/9/098104

## Interface states study of intrinsic amorphous silicon for crystalline silicon surface passivation in HIT solar cell

You-Peng Xiao(肖友鹏), Xiu-Qin Wei(魏秀琴), Lang Zhou(周浪)
Chin. Phys. B . 2017, 26(4): 048104 . **doi:** 10.1088/1674-1056/26/4/048104

## Influences of hydrogen dilution on microstructure and optical absorption characteristics of nc-$SiO_x$:H film

Zhao Wei, Du Lin-Yuan, Jiang Zhao-Yi, Yin Chen-Chen, Yu Wei, Fu Guang-Sheng
Chin. Phys. B . 2015, 24(10): 108102 . **doi:** 10.1088/1674-1056/24/10/108102

## Influences of hydrogen dilution on microstructure and optical absorption characteristics of nc-$SiO_x$:H film

Zhao Wei, Du Lin-Yuan, Jiang Zhao-Yi, Yin Chen-Chen, Yu Wei, Fu Guang-Sheng
Chin. Phys. B . 2015, 24(10): 108102 . **doi:** 10.1088/1674-1056/24/10/108102

---

# Influences of grain size and microstructure on optical properties of microcrystalline diamond films*

Jia-Le Wang(王家乐), Cheng-Ke Chen(陈成克), Xiao Li(李晓), Mei-Yan Jiang(蒋梅燕), and Xiao-Jun Hu(胡晓君)†

*College of Materials Science and Engineering, Zhejiang University of Technology, Hangzhou* 310014, *China*

(Received 2 September 2019; revised manuscript received 22 October 2019; accepted manuscript online 20 November 2019)

Microcrystalline diamond (MCD) films with different grain sizes ranging from 160 nm to 2200 nm are prepared by using a hot filament chemical vapor deposition (HFCVD) system, and the influences of grain size and structural features on optical properties are investigated. The results show that the film with grain size in a range of 160 nm–310 nm exhibits a higher refractive index in a range of (2.77–2.92). With grain size increasing to 620±300 nm, the refractive index shows a value between 2.39 and 2.47, approaching to that of natural diamond (2.37–2.55), and a lower extinction coefficient value between 0.08 and 0.77. When the grain size increases to 2200 nm, the value of refractive index increases to a value between 2.66 and 2.81, and the extinction coefficient increases to a value in a range of 0.22–1.28. Visible Raman spectroscopy measurements show that all samples have distinct diamond peaks located in a range of 1331 $cm^{-1}$–1333 $cm^{-1}$, the content of diamond phase increases gradually as grain size increases, and the amount of trans-polyacetylene (TPA) content decreases. Meanwhile, the $sp^2$ carbon clusters content and its full-width-at-half-maximum (FWHM) value are significantly reduced in MCD film with a grain size of 620 nm, which is beneficial to the improvement of the optical properties of the films.

**Keywords:** microcrystalline diamond films, grain size, microstructure, optical properties

**PACS:** 81.15.gh, 82.45.Mp, 82.75.Mj **DOI:** 10.1088/1674-1056/ab593d

## 1. Introduction

Diamond films have become increasingly attractive due to their excellent structural and unique optical properties, such as high optical transparency in the infrared region,[1] optically spin-sensitive transitions, and active quantum photonic centers.[2] These properties make diamond an ideal candidate for single-photon source applications in quantum sensing, quantum-optical characterization, *etc*.[3,4] In particular, a highly sensitive waveguide structure can be used in food safety inspection, designed for the analysis of proteins in different forms.[5,6] Diamond films are significantly used in opto-waveguide device and complex photonic integrated circuits technology due to its superb optical properties.[7] Optical constants, complex refractive index, and attenuation coefficient of light are essential parameters in the optical characterization of diamond materials.[8] Parameters with suitable opto-physical properties are critical to the further development of diamond-based biosensing waveguides.[9] Bulk diamond is easy to satisfy these requirements. However, it is very difficult and expensive to prepare, polish, and perform other processes on large-area single crystal diamond,[10] while nanocrystalline diamond (NCD) films are comprised mainly of nanocrystalline diamond grains and amorphous carbon, and exhibit local fluctuations in the dielectric function[11] and high optical transmission loss,[12] which will seriously degrade the device performance. Highly oriented and large grain size MCD film is better than the NCD film on the optoelectronic device serving as heat sink,[13] suggesting the advantage of MCD films as waveguide. High-quality polycrystalline diamond thin film photonic quantum technologies hold promise for repeating the success of integrated nanophotonic circuits and waveguide in non-classical applications.[14] Researchers have developed a miniaturized mid-IR spectroscopic measurement platform based on polycrystalline diamond strip waveguides to be able to demonstrate an ultra-sensitive, label-free detection of advanced chemical sensing/biosensing.[15,16] It suggests that the grain size of diamond is an important factor that can affect the optical properties. However, to the best of our knowledge, the description of complex refractive index of MCD films in different grain sizes has not yet been reported. The diamond nucleation rate, which determines the grain size to some extent, is controlled by the relative concentration of the carbon source, so we prepare diamond films with different grain sizes by adjusting the carbon source concentration.

In this paper, we prepare a series of MCD films with different grain sizes by using a hot filament chemical vapor deposition (HFCVD) system. The evolutions of complex refractive index of MCD films under a range of different grain sizes

*Project supported by the Key Project of the National Natural Science Foundation of China (Grant No. U1809210), the National Natural Science Foundation of China (Grant Nos. 50972129 and 50602039), the International Science Technology Cooperation Program of China (Grant No. 2014DFR51160), the National Key Research and Development Program of China (Grant No. 2016YFE0133200), the European Union's Horizon 2020 Research and Innovation Staff Exchange (RISE) Scheme (Grant No. 734578), the Belt and Road International Cooperation Project from Key Research and Development Program of Zhejiang Province, China (Grant No. 2018C04021), and the Natural Science Foundation of Zhejiang Province, China (Grant Nos. LQ15A040004 and LY18E020013).

†Corresponding author. E-mail: huxj@zjut.edu.cn

© 2020 Chinese Physical Society and IOP Publishing Ltd 

are investigated. With grain size in 160 nm, the refractive index reaches a value in a range of 2.83–2.98, because the film with smaller diamond crystals contains a larger percentage of surfaces atoms and larger percentage of interface, leading to worse optical properties. With average grain size increasing from 160 nm to 620 nm, the refractive index of MCD film decreases to a value in a range of 2.39–2.47, approaching to the value of natural diamond (2.37–2.55), and has the lowest extinction coefficient value (0.08–0.77). In this case, the value of full width at half maximum (FWHM) decreases to the lowest value (6.84 $cm^{-1}$), suggesting that less lattice defects exist in the MCD films. When the average grain size is 2100 nm, the refractive index increases to 2.66–2.81, which is in consistent with its microstructure deterioration. This proves that the reasonable grain size has an important significance for the applications in optical waveguide devices and biosensor.

## 2. Experiments methods

MCD films were prepared on a high-resistance single crystal silicon (10) substrate by using HFCVD. The carbon source was acetone ($CH_3COCH_3$), hydrogen was used to bring the acetone into the chamber and this part of hydrogen flow was named carbon source flow. The working pressure in the reaction chamber was 3.5 kPa, The substrate temperature fluctuated in a range of 840 °C–855 °C. The gas mixture consisted of $CH_3COCH_3$ and $H_2$. The extra added hydrogen flow rate was constant (200 sccm). The hot filament DC power was 2.4 kW. The as-deposited samples were prepared, respectively, with flow rates of carbon source of 40 sccm, 60 sccm, 80 sccm, and 100 sccm for 120 min, which are denoted as 3.5T40, 3.5T60, 3.5T80, and 3.5T100, respectively. The microstructures of the films were characterized by field emission scanning electron microscopy (FESEM, FEI nova450) and atomic force microscope (AFM Bruker Dimension). The phase composition of film was investigated by visible Raman spectrum measurements (Renishaw inva Reflex) with an excitation wavelength of 532 nm at room temperature. The optical process was analyzed by spectroscopic ellipsometry (GES-5E) instrument with a wavelength range of 400 nm–2000 nm and measuring angle close to the Brewster angle of $6^\circ \pm 0.1^\circ$. There are equations which describe the optical constant building and fitting by Cauchy model[17]

$$n(\lambda) = A + B/\lambda^2 + C/\lambda^4, \tag{1}$$

$$K(\lambda) = \alpha \exp\left\{\beta\left[12400\left(\frac{1}{\lambda} - \frac{1}{\gamma}\right)\right]\right\}, \tag{2}$$

where $A$, $B$, and $C$ refer to the material-related constants, $\alpha$ represents the extinction coefficient amplitude, $\beta$ is the exponential factor, and $\gamma$ is the band gap.

## 3. Results and discussion

Figure 1 shows the surface morphologies of the pristine-MCD films. It is observed that all samples possess well continuity and compact structures without disfigurement such as holes. The grain size increases with carbon source concentration increasing. When the film is completely continuous, the grain volume follows the improvement of van der Drift, which means that larger grains inhibit the growth of adjacent smaller grains.[18] With the average diameter exceeding 100 nm, the film becomes a microcrystal instead of a nanocrystal,[19] and the particle size distributions of the samples 3.5T40, 3.5T60, 3.5T80, and 3.5T100 are shown on the right of Fig. 1. The average crystallite sizes are $\sim 160 \pm 50$ nm, $310 \pm 100$ nm, $620 \pm 300$ nm, and $2200 \pm 900$ nm for samples 3.5T40, 3.5T60, 3.5T80, and 3.5T100, respectively. The diamond grain orientations of the film are mainly in (100) and (110) planes. In addition, the FESEM results show that the uniformity of crystal size distribution is enhanced by the high-concentration carbon source, leading to the full growth of the grain boundaries (GBs).

Theoretically, the refractive index of the material changes with the variation of wavelength, so the optical performance is a function of wavelength variation.[20–22] For this purpose, we use spectroscopic ellipsometry (SE) to investigate the optical properties of MCD films over the spectral wavelength range of 380 nm–1000 nm. The structural characteristics of the diamond film are affected by deposition conditions, such as temperature, growth rate, ion assist, pressure, *etc*.[23] Meanwhile, ellipsometry cannot directly measure the optical properties of the film. Therefore, characterizing optical constants of the films with different grain sizes requires fitting a data model to extract sample information. According to Fresnel formula,[24,25]

$$r_\mathrm{p} = \frac{n_2\cos\theta_1 - n_1\cos\theta_2}{n_2\cos\theta_1 + n_1\cos\theta_2} = \frac{\tan(\theta_1 - \theta_2)}{\tan(\theta_1 + \theta_2)}, \tag{3}$$

$$r_\mathrm{s} = \frac{n_1\cos\theta_2 - n_2\cos\theta_1}{n_1\cos\theta_2 + n_2\cos\theta_1} = \frac{\tan(\theta_2 - \theta_1)}{\tan(\theta_2 + \theta_1)}, \tag{4}$$

when light is oriented in the plane of the medium, the linear polarization consists of parallel components $r_\mathrm{p}$ and vertical components $r_\mathrm{s}$. Where the parameters $\theta_1$ and $\theta_2$ are the incident angle and the refractive angle, respectively. $n_1$ and $n_2$ are the complex refractive index of air and the one of the films, respectively. They are related to the complex reflectance ratio $\rho$ of the polarized light by the equations

$$\rho = \tan(\Psi)\,\mathrm{e}^{\mathrm{i}\Delta} = \frac{r_\mathrm{p}}{r_\mathrm{s}}. \tag{5}$$

In order to describe this polarization change of light reflecting, we introduce the amplitude ratio ($\Psi$) and phase shift ($\Delta$) to construct an optical model fitting measured ($\Psi$, $\Delta$) spectra.[26]

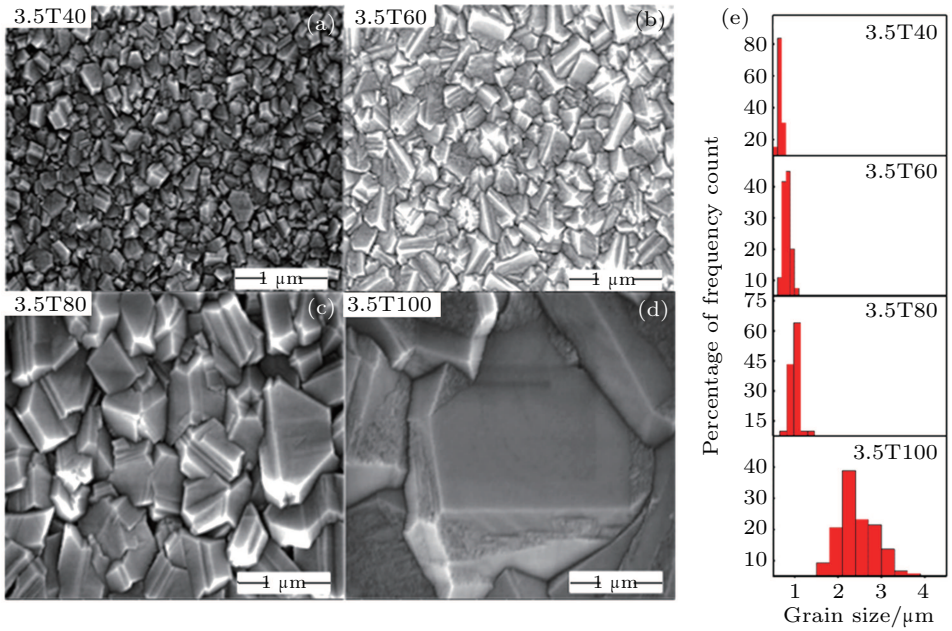



**Fig. 1.** FESEM graphs of diamond films of (a) 3.5T40, (b) 3.5T60, (c) 3.5T80, and (d) 3.5T100, respectively. (e) Particle size distributions of samples 3.5T40, 3.5T60, 3.5T80, and 3.5T100.

Figure 2 shows that the optical constants of films in a wavelength range of 400 nm–2000 nm describes the values of fitting parameters in the SE data analysis process by describing the refractive index ($n$) and extinction coefficient ($k$) curve shapes through the Cauchy model and the dispersion equation. The smoothed $n$–$k$ spectral curve is obtained by describing the optical function through using equation parameter. Figure 2(a) shows that the refractive index values of MCD films with different flow rates of carbon source in a wavelength range of 400 nm–2000 nm. The refractive indices of the MCD films are in ranges of 2.83–2.98, 2.77–2.92, 2.39–2.47, and 2.66–2.81 for samples 3.5T40, 3.5T60, 3.5T80, and 3.5T100, respectively. It is also observed that the refractive index of sample 3.5T80 is similar to that of natural diamond with a value in a range of 2.37–2.55[12] as compared with those of samples synthesized under other carbon source concentration.

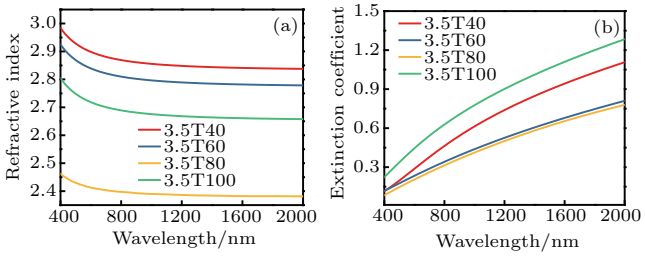



**Fig. 2.** (a) Measured refractive index *versus* wavelength. (b) Extinction coefficient *versus* wavelength of different samples.

As is well known, the value of the imaginary part represents the extinction coefficient, and figure 2(b) shows the fitting result of the index extinction coefficient of the MCD film. It indicates that the index extinction coefficients of the thin films are in a range of 0.11–1.12, 0.12–0.81, 0.08–0.77, and 0.22–1.28 for samples 3.5T40, 3.5T60, 3.5T80, and 3.5T100, respectively. It is obvious that the extinction coefficient gradually increases with wavelength increasing. The extinction coefficient is related to the absorption coefficient and is an important parameter to characterize the attenuation of light energy. It is observed from Fig. 2(b) that the sample 3.5T80 also has the lowest extinction coefficient in a range of 0.08–0.77, indicating that the optical absorption rate thereof also decreases. This suggests that the grain size of $\sim$ 620 nm is favorable for improving the optical transmittance of the film.

In order to further characterize the microscopic morphology of the MCD films, we use AFM to characterize the four samples in two dimensions and three dimensions to visualize the roughness and microstructure information of the film surface as shown in Fig. 3. Listed in Table 1 are average roughness ($R_a$) and root-mean-square roughness ($R_q$) for these samples. The results show that the average roughness and grain size for each of diamond films increase with flow rate of carbon source increasing to 100 sccm.

**Table 1.** Results of AFM analysis for samples.

| Sample | $R_a$/nm | $R_q$/nm | Mean grain size/nm |
|---|---|---|---|
| 3.5T40 | 10.5 | 13.8 | 160 |
| 3.5T60 | 22.0 | 30.3 | 310 |
| 3.5T80 | 333.0 | 407.0 | 620 |
| 3.5T100 | 1310.0 | 1560.0 | 2200 |

Figures 3(A) and 3(a) show that very small particles form a large one, which does not exhibit the characteristic of crystallinity in an average grain size of 160 nm. Its $R_a$ and $R_q$ values are as low as 10.5 nm and 13.8 nm, respectively. This indicates that small grain size exhibits a low level of surface roughness. As shown in Figs. 3(B) and 3(b), the gaps between

particles gradually begin to narrow and the crystallinity of particles to increase gradually. $R_a$ and $R_q$ values also increase to about 22.0 nm and 30.3 nm, respectively. As shown in Figs. 3(C) and 3(c), with the grain size increasing to 620 nm, the grains have excellent uniformity, and the diamond GBs are refined. It is observed that from Figs. 3(D) and 3(d), as the grain size further increases to 2200 nm, there is a deep gully between the crystal grains, and the grain boundaries are very obvious. By combining the results in Table 1, we reveal that $R_a$ value increases from 333 nm to 1310 nm and the $R_q$ value increases from 407.0 nm to 1560.0 nm. This indicates that the large grain size has high surface roughness and root-mean-square roughness. It is also revealed that there exists a transition grain size of 620 nm, above which the diamond crystallinity degree improves.

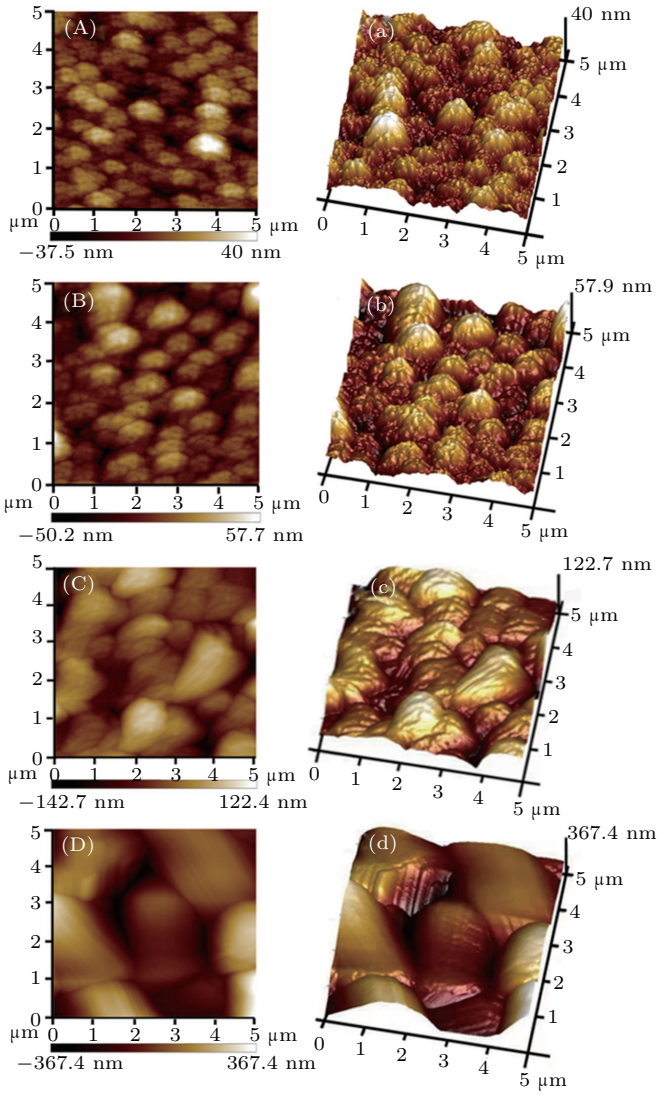



**Fig. 3.** Two-dimensional (2D) and three-dimensional (3D) AFM images of samples: (A) and (a) 3.5T40, (B) and (b) 3.5T60, (C) and (c) 3.5T80, (D) and (d) 3.5T100.

To understand the origin of the optical properties, we perform visible Raman spectrum measurements in a range of 1000 $cm^{-1}$–1800 $cm^{-1}$ to characterize the phase composition evolutions of the samples as shown in Fig. 4(a). The spectra were well fitted with six Gaussian–Lorentzian peaks by using OriginPro9.0 software. The fitted peaks in a range of about 1332 $cm^{-1}$–1334 $cm^{-1}$ are attributed to diamond phase,[27,28] while the fitted peaks in ranges of 1340–1360 and 1560 $cm^{-1}$–1580 $cm^{-1}$ are due to reflection of the D and G bands of $sp^2$-bonded carbon,[28,29] respectively. In addition, the spectra of the films have peaks in ranges of about 1140 $cm^{-1}$–1180 $cm^{-1}$ and 1470 $cm^{-1}$–1490 $cm^{-1}$, which are related to bending and stretching vibrations of trans-polyacetylene (TPA) at the GBs of the MCD films,[30] respectively. Moreover, as the flow rate of carbon source increases, the TPA peak gradually weakens and disappears, while the diamond peak intensity increases.

Figure 4(b) shows the evolutions of the diamond phase content at different flow rates of carbon sources, which are calculated by the fitted peak area of the diamond peak and other non-diamond peaks in Fig. 4(b) according to the formula in Ref. [31]. It is observed that diamond phase content accounts for 91.7%, 91.3%, 94.2%, and 95.8% with the grain size increasing because larger grain size corresponding to fewer GBs, which is consistent with the results of Figs. 1(a)–1(d).

As shown in Fig. 4(c), our calculated integrated area ratio of the TPA peaks (1140 $cm^{-1}$ and 1470 $cm^{-1}$) to all peaks characterizes the intensity of peaks $I_{TPA}/I_{SUM}$ values from visible Raman spectra, and the TPA content decreases with grain size increasing. When the flow rate of carbon source increases to 80 sccm, the TPA content significantly decreases to 0.98%. The decrease of TPA content implies that there is a desorption process for hydrogen in the film. For TPA existing in amorphous carbon GBs, the decrease of TPA indicates the decreasing of GBs.[3,32] This reveals that the increasing of grain size is beneficial to reducing the content of amorphous carbon GBs.

Figure 4(c) also shows the intensity ratio of the D peak value to G peak value ($I_D/I_G$) from Fig. 4(a). In general, the area intensity ratio of the D and G peaks ($I_D/I_G$) is thought to be proportional to the number of aromatic rings in the $sp^2$-bonded carbon clusters and it provides an estimation of the ordering and the number of $sp^2$-bonded carbon clusters.[33,34] The $I_D/I_G$ value as a function of flow rate of carbon source shown in Fig. 4(b) obviously becomes the lowest value (0.51) in 80 sccm and then it increases to 1.57 with the flow rate of carbon source increasing to 100 sccm. This indicates that the number of aromatic rings increases and the number of $sp^2$ interface defects increases with the grain size further increasing.[35]

The FWHM value can be used to effectively characterize the crystal quality information of the MCD film.[3] Figure 4(d) shows the dependence of the FWHM value of the diamond and G peaks on flow rate of carbon source. For samples of 3.5T40

and 3.5T60, FWHM value of diamond peak slightly decreases from 8.21 $cm^{-1}$ to 8.15 $cm^{-1}$. With the grain size further increasing to 620 nm, the diamond peak FWHM value dramatically decreases to 6.84 $cm^{-1}$, which is much smaller than that of sample 3.5T100 (10.59 $cm^{-1}$). This indicates that the quality of diamond grains in sample 3.5T80 is better than that of samples 3.5T40, 3.5T60, and 3.5T100, revealing that the diamond in 3.5T80 with a grain size of 620 nm has the highest quality.

In this study, for samples of 3.5T40, the G band FWHM value is 73.06 $cm^{-1}$. With the grain size increasing to 310 nm, the G band FWHM value increases from 73.06 $cm^{-1}$ to 99.43 $cm^{-1}$. This indicates that the graphitic clusters become more disorder and $sp^2$ configuration transforms from olefinic group into a ring structure.[36] However, as the grain size increases to 620 nm, the G band FWHM value turn into 60 $cm^{-1}$, implying that the quality of diamond grain is better than that of samples 3.5T40 and 3.5T60. For the sample 3.5T100, the G band FWHM value is 101.97 $cm^{-1}$. This means that with the grain size further increasing, the MCD film can produce a greater number of ring structures of the $sp^2$ configuration and turn more disordered.

Considering all the Raman information, we can see that several possible factors affect optical performance. For the samples 3.5T40 and 3.5T60, as the average grain size increases from 160 nm to 310 nm, the refractive index range increases from 2.83–2.98 to 2.77–2.92, implying that the optical performance is improved mainly due to the increase of diamond grain size. For the sample of 3.5T80 with the average grain size of 620 nm, the $I_D/I_G$ value decreases to the lowest value (0.51), and the FWHM values of its diamond and G bonds are smaller than those of other samples, indicating that the quality of diamond grains in sample 3.5T80 is better than that of other samples, revealing that not only the grain size but also the good crystal quality will dramatically improve the optical properties. However, with the grain size further increasing to 2100 nm, the FWHM value of $I_D/I_G$ and G band of sample 3.5T100 increase and its refractive index value is lower than those of samples 3.5T40 and 3.5T60, which further proves that the optical properties will be improved by increasing the grain size for each of MCD film, and also affected by microstructural evolution.

On the other hand, the grain size gradually increases with the flow rate of carbon source increasing in a range of 40 sccm–100 sccm. The results show that the flow rate of carbon source has an effect on the surface nucleation density of MCD film. The nucleation density is quite low as the flow rate of carbon source is lower than 80 sccm, and does not exhibit the characteristic of crystallinity. When the flow rate of carbon source is 80 sccm (with the average grain size of 620 nm), hydrogen atoms meet an optimal etching rate, and the film nucleation density is larger and compact. Also, GBs are refined and the crystallinity is improved more dramatically than those in samples 3.5T40 and 3.5T60. Meanwhile, the sample 3.5T80 has the lowest value of $I_D/I_G$ and its refractive index value is close to the natural diamonds, suggesting that the suitable grain size can reduce the $sp^2$ carbon content and optimize the lattice structure, which greatly improves the optical properties.

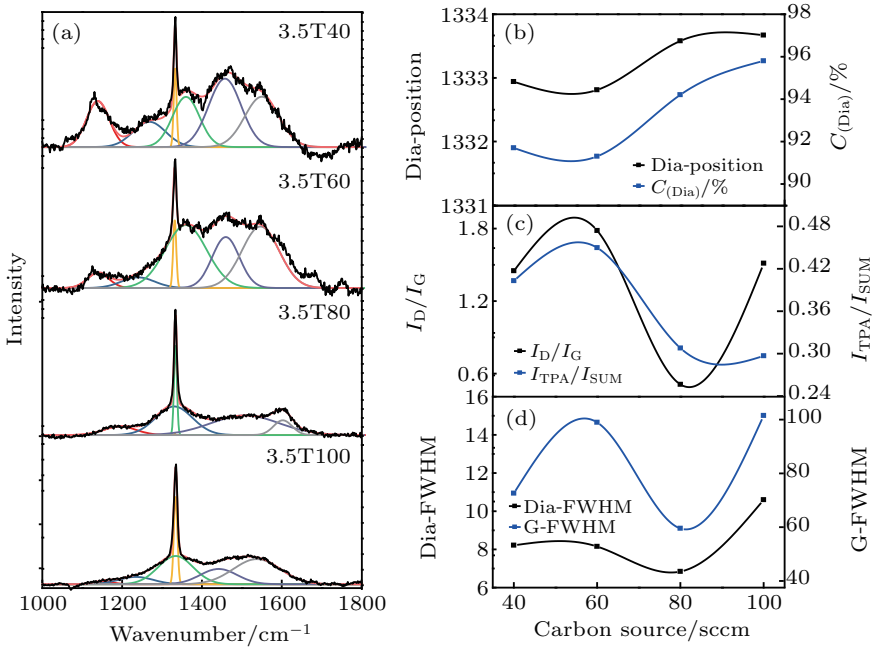



**Fig. 4.** (a) Typical visible Raman spectra of MCD films prepared under different carbon source conditions, (b) diamond peak position and its content *versus* carbon source flow rate, (c) ratio of $I_{TPA}/I_{SUM}$ and $I_D/I_G$ value *versus* carbon source flow rate, (d) G and diamond band position and its FWHM values on different grain sizes *versus* carbon source flow rate.

## 4. Conclusions

In this work, we successfully prepar a series of MCD films with different grain sizes on silicon wafer substrates by adjusting the flow rate of carbon source concentration in the CVD process. Based on the results obtained by FESEM, AFM, Raman spectroscopy, and SE, the effects of diamond grain size films on the composite refractive index properties are investigated. The results show that the sample synthesized at 80 sccm has better properties of complex refractive index. Particles having an average particle size of about 620 nm are uniformly distributed on the surface of the silicon wafer. In the condition, the $sp^2$ carbon content and the residual stress in the film are greatly reduced, and the quality of diamond grains is improved. The refractive index value fluctuates from 2.39 to 2.47. When the flow rate of carbon source is lower than 80 sccm, the average grain size value is less than 300 nm, Raman spectra show that non-diamond phase content increases, and the number of aromatic rings and $sp^2$ carbon content increase in GBs, which increases the refractive index value of the film. When the flow rate of carbon source is greater than 80 sccm, the average grain size increases to 2200 nm. In this case, the number of $sp^2$ carbon clusters at GBs increases significantly from 0.51 to 1.51 and its crystal quality decreases. The range of refractive index value increases from 2.39–2.47 to 2.66–2.81, which is a disadvantage for obtaining a good refractive-index film.

## References


[1] Checoury X, Neel D, Boucaud P, Gesset C, Girard H, Saada S and Bergonzo P 2012 *Appl. Phys. Lett.* **101** 171115

[2] Hoi B D, Yarmohammadi M and Kazzaz H A 2017 *J. Magn. Magn. Mater.* **439** 203

[3] Mei Y S, Fan D, Lu S H, Shen Y G and Hu X J 2016 *J. Appl. Phys.* **120** 225107

[4] Chen Y, Lee C, Lu L, Liu D, Wu Y K, Feng L T, Li M, Rockstuhl C, Guo G P, Guo G C, Tame M and Ren X F 2018 *Optica* **5** 1229

[5] Piron P, Catalan E V, Haas J, Osterlund L, Nikolajeff F, Andersson P O, Bergstrom M J, Mizaikoff B and Karlsson M 2018 *Photonic Instrumentation Engineering* V, eds. Soskind Y G and Olson C (Bellingham: Spie-Int Soc Optical Engineering)

[6] Wrachtrup J and Jelezko F 2006 *J. Phys.-Condes. Matter* **18** S807

[7] Gao F, Van Erps J, Huang Z H, Thienpont H, Beausoleil R G and Vermeulen N 2018 *IEEE J. Sel. Top. Quantum Electron.* **24** 6100909

[8] Struk P 2019 *Materials* **12** 175

[9] Qi Y P, Zhang X W, Zhou P Y, Hu B B and Wang X X 2018 *Acta Phys. Sin.* **67** 197301 (in Chinese)

[10] Doronin M A, Polyakov S N, Kravchuk K S, Molchanov S P, Lomov A A, Troschiev S Y and Terentiev S A 2018 *Diam. Rel. Mater.* **87** 149

[11] Remes Z, Babchenko O, Varga M, Stuchlik J, Jirasek V, Prajzler V, Nekvindova P and Kromka A 2016 *Thin Solid Films* **618** 130

[12] Sobaszek M, Skowronski L, Bogdanowicz R, Siuzdak K, Cirocka A, Zieba P, Gnyba M, Naparty M, Golunski L and Plotka P 2015 *Opt. Mater.* **42** 24

[13] Ajikumar P K, Ganesan K, Kumar N, Ravindran T R, Kalavathi S and Kamruddin M 2019 *Appl. Surf. Sci.* **469** 10

[14] Rath P, Kahl O, Ferrari S, Sproll F, Lewes-Malandrakis G, Brink D, Ilin K, Siegel M, Nebel C and Pernice W 2015 *Light: Sci. & Appl.* **4** e338

[15] Malmstrom M, Karlsson M, Forsberg P, Cai Y X, Nikolajeff F and Laurell F 2016 *Opt. Mater. Express* **6** 1286

[16] Wang X F, Karlsson M, Forsberg P, Sieger M, Nikolajeff F, Osterlund L and Mizaikoff B 2014 *Anal. Chem.* **86** 8136

[17] Raja Shekar P V, Madhavi Latha D and Pisipati V G K M 2017 *Opt. Mater.* **64** 564

[18] Delfaure C, Tranchant N, Mazellier J P, Ponard P and Saada S 2016 *Diam. Rel. Mater.* **69** 214

[19] Mistrik J, Janicek P, Taylor A, Fendrych F, Fekete L, Jager A and Nesladek M 2014 *Thin Solid Films* **571** 230

[20] Ficek M, Sobaszek M, Gnyba M, Ryl J, Gołuński Ł, Smietana M, Jasiński J, Caban P and Bogdanowicz R 2016 *Appl. Surf. Sci.* **387** 846

[21] Bogdanowicz R, Sobaszek M, Sawczak M, Grigorian G M, Ficek M, Caban P, Herman A and Cenian A 2019 *Diam. Rel. Mater.* **96** 198

[22] Khomich A V, Kovalev V I, Zavedeev E V, Khmelnitskiy R A and Gippius A A 2005 *Vacuum* **78** 583

[23] Hilfiker J N, Pribil G K, Synowicki R, Martin A C and Hale J S 2019 *Surf. Coat. Technol.* **357** 114

[24] Abdel-Wahab F, Ashraf I M and Montaser A A 2019 *Optik* **178** 813

[25] Zhu J, Han J, Han X, Meng S, Liu A and He X 2006 *Opt. Mater.* **28** 473

[26] Aghgonbad M M and Sedghi H 2018 *Chin. J. Phys.* **56** 2129

[27] Kuntumalla M K, Elfimchev S, Chandran M and Hoffman A 2018 *Thin Solid Films* **653** 284

[28] Huang K, Hu X, Xu H, Shen Y and Khomich A 2014 *Appl. Surf. Sci.* **317** 11

[29] Haubner R and Rudigier M 2013 *Phys. Procedia* **46** 71

[30] Xu H, Chen C, Fan D, Jiang M, Li X and Hu X 2019 *Carbon* **145** 187

[31] Sails S R, Gardiner D J, Bowden M, Savage J and Rodway D 1996 *Diam. Rel. Mater.* **5** 589

[32] Fan L S, Constantin L, Li D W, Liu L, Keramatnejad K, Azina C, Huang X, Golgir H R, Lu Y, Ahmadi Z, Wang F, Shield J, Cui B, Silvain J F and Lu Y F 2018 *Light-Sci. Appl.* **7** 17177

[33] Xu H, Liu J J, Ye H T, Coathup D J, Khomich A V and Hu X J 2018 *Chin. Phys. B* **27** 096104

[34] Gu S S and Hu X J 2013 *J. Appl. Phys.* **114** 023506

[35] Ferrari A C and Basko D M 2013 *Nat. Nanotechnol.* **8** 235

[36] Ferrari A C and Robertson J 2000 *Phys. Rev. B* **61** 14095